16th World Conference on Earthquake Engineering, 16WCEE 2017
Santiago Chile, January 9th to 13th 2017
Paper N° 1499
Registration Code: S-O1464414238

Unexpected fluctuation in seismic response accompanied by model uncertainty in numerical simulation

K. Iiyama[(1)], H. Morikawa[(2)], S. Hirose[(3)]

[(1)] *Researcher, Tokyo Institute of Technology, iiyama.k.aa@m.titech.ac.jp*
[(2)] *Professor, Tokyo Institute of Technology, morika@enveng.titech.ac.jp*
[(3)] *Professor, Tokyo Institute of Technology, hirose.s.aa@m.titech.ac.jp*

Abstract

The focus of this paper is the unexpected fluctuation found in the seismic response due to a slight difference in the settings of structural parameters. Over the past few decades, the performance of computers has improved considerably, and simulation-based techniques with a large mass of information on objective structures can easily be applied to damage evaluations, hazard assessments, and so on. For simulation-based techniques, the numerical models must be set appropriately. Thus, design parameters or other equivalent values for the targeted structures are often incorporated into the numerical models, although it is known that there are certain discrepancies between the design parameters and the actual properties of existing structures. Since the numerical results necessarily fluctuate according to these discrepancies, a kind of "uncertainty" should be taken into account for the structural parameters and for the corresponding responses in order to ensure the reliability of the numerical results. Although it is still quite a task to determine the uncertainty of structural parameters quantitatively, examining the statistical properties of the fluctuation in seismic response caused by certain gaps in the structural parameters is of significant importance.

To statistically examine the fluctuation properties of the seismic response, a large number of numerical tests were conducted using several numerical models of the common type and various input earthquakes. This study employed models with single- and multi-degrees of freedom that were modeled by shear-spring masses. The skeletons of the shear springs were modeled by normal bilinear or trilinear types, that are generally applied to concrete structures, base-isolated members, and so on. The yield force and the elastic period were taken as the input structural parameters in this study because the performance of structures can be clearly determined with them and they have a direct effect on the seismic response. The maximum story drift angle was taken as the response quantity, as it is an important factor for evaluating the damage level when building structures. To discuss the fluctuation in seismic response accompanied by slight changes in the yield force and the natural period, the maximum gap between the maximum story drift angles for the corresponding yield force and natural period within a certain band, was examined under several combinations of structural properites and various input earthquakes.

Introducing the ratio of fluctuation, Rf_j, as an evaluation index, the statistical properties of the seismic response were summarized as follows: 1) The mean of Rf_j with a slight change in the yield force highly depends on the ductility level. 2) The mean of Rf_j with a slight change in the natural period of structures depends more on the natural period than on the ductility level. 3) A slight difference in structural parameters, for instance, 2% in yield force or 0.01 s in natural period, may possibly cause a difference in the maximum story drift angle of around 10%. 4) Rf_j agrees well with the beta distribution.

Keywords: Seismic response analysis, Model uncertainty, Mass model, Story drift angle, Ductility

1. Introduction

When a great earthquake disaster strikes a large city, minimizing the damage expansion is always an important issue. Various techniques to predict the possible loss of human lives and material damage have been proposed and developed, for instance, the probabilistic seismic hazard analysis (PSHA)[1),2)], fragility curves[3),e.g.], and national seismic hazard maps[4)] are popular ones. On the other hand, the performance of computers has considerably improved in recent years and simulation-based techniques are more attractive and more practical for use as damage assesment tools than old empirical methods if reliable information on the structural parameters of the objective structures can be introduced into the numerical model. For instance, the integrated earthquake simulator (IES)[5)] is one of the powerful tools for conducting inclusive damage investigations or safety evaluations in target areas[6)] for the seismic response of not only a large number of buildings, but also large-scale continuous infra-structures, human action during evacuations, and so on.

With such a numerical simulation, the setting (or assuming) of many structural properties for the objective structure is necessary in order to quantitatively estimate its response and evaluate its safety. As a matter of course, the structural properties should be assumed rationally because they govern the seismic behavior of the structure. In most cases, the design parameters, or the other equivalent values of the targeted structure, are introduced as the analytical conditions. However, the parameters do not necessarily correspond to the current state of existing buildings. In other words, there are some discrepancies between the design parameters and the actual parameters. Thus, a kind of "uncertainty" should be taken into account for structural parameters and the corresponding responses to ensure the reliability of the numerical results. Considering the difficulty in determining the uncertainty of structural parameters, this study examined the statistical properties of the fluctuation in seismic response caused by certain gaps in the structural parameters.

To statistically examine the properties of fluctuation in the seismic response, a large number of numerical tests were conducted using simple and general types of numerical models and various input earthquakes. This study employed models with single- and multi-degrees of freedom that were modeled by shear-spring masses. The skeletons of the shear springs were modeled by normal bilinear or trilinear types, that are generally applied to concrete structures, base-isolated members, and so on. The yield force and the elastic period were taken as the input structural parameters in this study because the performance of structures can be clearly determined with them and they have a direct effect on the seismic response. The maximum story drift angle was taken as the response quantity, which is an important factor when building structures. To discuss the fluctuation in the seismic response accompanied by slight changes in the yield force and the natural period, the possible gaps in the maximum story drift angle within certain bands of the yield force and the natural period were calculated for several combinations of structural properites and various input earthquakes.

2. Analytical conditions and evaluation method

2.1 Fluctuation in numerical values in seismic analysis

Let X be one of the structural properties and Y be the seismic response or the corresponding damage index. Figure 1 shows a diagrammatic sketch of the relationship between X and Y; $Y=g(X)$. In the figure, the symbol j represents a discrete point of X and ΔX_j indicates the width of the j-th band within X. Y_{jmax} and Y_{jmin} denote the maximum and the minimum response values within ΔX_j, respectively. The figure on the left is an example of the case in which Y changes in an inversely proportional way to X, but the change is comparatively stable. In such a case, the gap between the response values is small or predictable for the narrow band of ΔX_j. For complicated nonlinear analyses, however, Y often fluctuates in an unstable manner, as shown in the figure on the right. The numerical response then takes unexpected values even if the width of ΔX_j is narrow. Such a gap in Y, that is, $|Y_{jmax}-Y_{jmin}|$, possibly affects the reliability of the assessment based on the numerical simulation. Considering these points, a stochastic method should be introduced into the simulation or a proposition should be assumed whereby the numerical results take values within a certain range. Although it is a great task to generalize the possible range quantitatively, the characteristics can be examined statistically by introducing a large number of numerical tests.

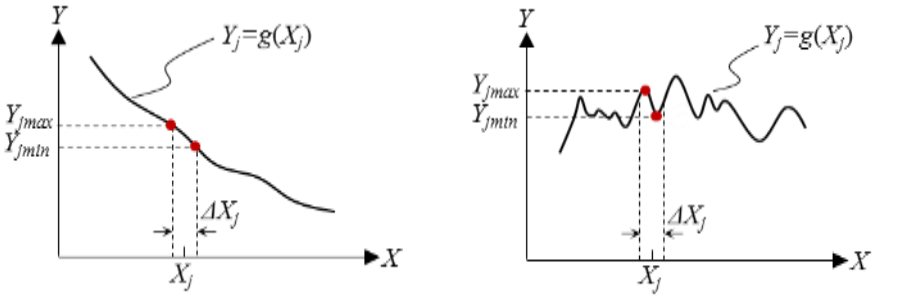

(a) Relatively stable but sensitive (b) Unstable and relatively insensitive

Fig. 1 – Diagrammatic sketch of relationship between *X* and *Y*

2.2 Model settings and analytical cases

To examine the characteristics of fluctuation statistically, several types of numerical models and various input earthquakes were employed in this study. The numerical models and analytical conditions for the calculation are as follows: As a basic model, shear-spring mass models which have an *n* degree-of-freedom (*n*DOF) for one direction were employed in this study. The skeletons of the story stiffness were set by normal bilinear or trilinear types, as shown in Fig. 2, because these skeletons are generally applied to concrete structures, base-isolated members, and so on. An example of the model is shown in Fig. 2. The model has the same story mass *M*, and the *j*-th story stiffness K_j is designed to satisfy the Ai-distribution that is adjusted to the targeted elastic period (T_1). The model damping factor of 3.0% is considered. For $n > 1$, Rayleigh damping is applied as the viscous damping matrix using a damping factor of 3.0% for the first and second modes. Newmark's beta method with the time interval of dt=0.001 s was applied. γ is the ratio of the yield stiffness K_{jy} to the initial stiffness K_{je}.

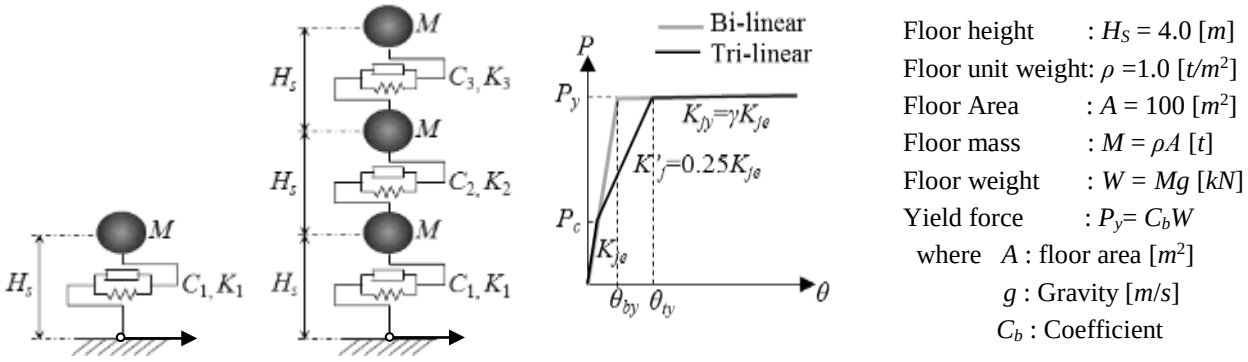

<1DOF model> <3DOF model> <Skeleton of shear spring> <Structural properties>

Fig. 2 – Model settings

Two structural properties were selected here as *X*. They are coefficient C_b (=P_y/W), instead of yield force P_y, and the elastic period of the structure (T_1), because the structure's performance can be clearly determined and they have a direct effect on the seismic response. As seismic response *Y*, the maximum story drift angle of the structure, θ_{max}, is used ($Y=\theta_{max}$). As for *X*, the following ranges are considered in the calculation:

$$X=C_b\ [-]\ :\ 0.1 \le X \le 0.9\ ,\ dX=0.02\ \ (N_{Cb}=41)$$

$$X=T_1\ [\mathrm{s}]\ :\ 0.05 \le X \le 0.45,\ dX=0.01\ (N_{T1}=41)$$

where symbol *dX* denotes the interval of discretized $X=X_j$, and N_{Cb} and N_{T1} are the numbers of discretization points existing within the above ranges, respectively. Table 1 shows the analytical conditions for the calculation, where superscript *t* of p_1 denotes the earthquake number. As the total number of the artificial waves and the observed waves are respectively 886 and 1189, namely, *t* takes values from 1 to 886 for $p_1{}^t$=1, and to 1189 for $p_1{}^t$=2. One numerical simulation (for one input earthquake) was conducted for 1681 (=$N_{Cb}\times N_{T1}$) combinations of

C_b and T_1 for the condition $\{P\}=\{p_1^t, p_2, p_3, p_4, p_5\}$. p_i takes the value of 1 or 2. For example, $\{P\}=\{1,2,2,1,1\}$ indicates that the conditions of "the artificial wave" and "the 3DOF-bilinear model with γ=0.01" are applied. Consequently, 886 calculations are conducted by using all artificial waves. The total number of patterns in $\{P\}$ is 32 ($=_2C_1^5$) and this study took only 24 cases, except for the case of $\{p_1^t, p_3\}=\{1, 2\}$. (The number of patterns for $\{p_1^t, p_3\}=\{1, 2\}$ is $_2C_1^3$.) From the numerical study using a large number of input waves, a sufficient number of response values was obtained and the statistical properties of the response are herein discussed.

Table 1 – Conditions for calculation

Condition's No.	p_1^t < Input >	p_2 < DOF >	p_3 < $\gamma = K_{je}/K_{jy}$ >	p_4 Skeleton	p_5 ΔX
1	Artificial waves*	1	0.001	Bilinear	dX
2	Observed waves**	3	0.01	Trilinear	$5dX$

* Scenario earthquake "Nankai Trough" by the Cabinet Office, Government of Japan; The total number of waves is 886.
** Records observed during the 2011 Tohoku Earthquake (http://www.kyoshin.bosai.go.jp/kyoshin/); The total number of waves is 1189.

2.3 Evaluation index

From one numerical simulation, 1681 ($=N_{Cb}\times N_{T1}$) values for θ_{max} can be calculated, as shown on the left graph of Fig. 3. The simulation is conducted for all objective waves, accordingly, 886 graphs are obtained when p_1^t=1, and 1189 ones are obtained when p_1^t=2. To examine the statistical properties of the gaps of θ_{max} within the j-th band, ΔX_j, the following index is introduced as the response quantity. The ratio of fluctuation, $Rf_j^{s,t}$, is a function of X_j and the maximum ductility μ_{ymax} under the condition of w^s and p_i (i=1,..,5, shown in Table 1). Variables μ_{ymax} and w^s are explained below.

$$Rf_j^{s,t}(X_j, \mu_{y\max} \mid w^s, p_1^t, p_2, p_3, p_4, p_5) = \frac{\left|\theta_{j\max} - \theta_{j\min}\right|}{\theta_{j\max}} \quad (\because\ 0 \le Rf_j^{s,t} \le 1) \tag{1}$$

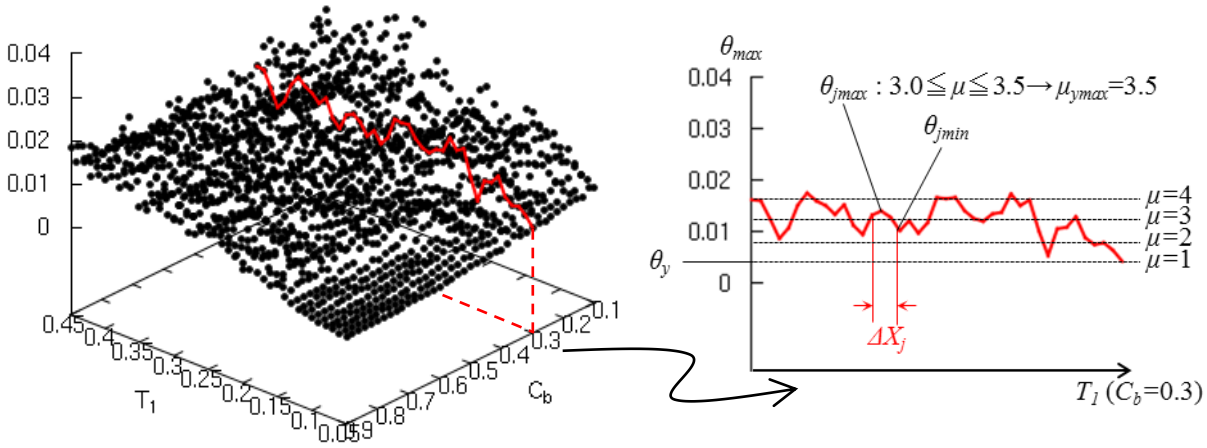

Fig. 3 – Outline of calculation process of Rf_j

For instance, in the case of $X=T_1$, the $Rf_j^{s,t}$ is calculated on all lines of $C_b=w^s$ (w^s = 0.1+0.02(s−1), s=1,2,…,41 ∵ $0.1 \le C_b \le 0.9$ and dC_b=0.02) for each band of ΔX_j, for all j in the range of $0.05 \le T_1 \le 0.45$ (dT_1=0.01). The total number of ΔX_j for each line of $C_b=w^s$ is 40 for p_5=1 and 36 for p_5=2, respectively. Likewise, in the case of $X=C_b$, the $Rf_j^{s,t}$ is calculated on all lines of $T_1=w^s$ (w^s = 0.05+0.01(s−1), s=1,2,…,41 ∵ $0.05 \le T_b \le 0.45$ and dT_1=0.01) for each band of ΔX_j, for all j in the range of $0.1 \le C_b \le 0.9$ (dC_b=0.02). The total number of ΔX_j for each line of $T_1=w^s$ is 40 for p_5=1 and 36 for p_5=2, respectively. In addition, ductility is possibly one of the factors which affects Rf_j. Hence, the calculated Rf_j was classified into each scale of μ according to the scale of μ_{ymax} within ΔX_j.

$$\mu_{y\max} = \frac{\theta_{j\max}}{\theta_y} \tag{2}$$

In this study, the scale of μ_{ymax} was discretized to 0.5 and the cases of μ_{ymax}>8 were omitted. This means that the scale of μ_{ymax} was classified to 16 levels. To explain the statistical characteristics of $Rf_j^{s,t}$, the mean and the standard deviation of $Rf_j^{s,t}$ were calculated for each combination of X_j and μ_{ymax} as follows:

$$Rf_{jAve}(X_j, \mu_{y\max} | \{P\}) = \frac{1}{N_{st}} \sum_s \sum_t Rf_j^{s,t}(X_j, \mu_{y\max} | w^s, p_1^t, p_2, p_3, p_4, p_5) \quad for\ N_{st} \neq 0 \tag{3}$$

$$Rf_{jStd}(X_j, \mu_{y\max} | \{P\}) = \sqrt{\frac{1}{N_{st}} \sum_s \sum_t \left\{Rf_j^{s,t}(X_j, \mu_{y\max} | w^s, p_1^t, p_2, p_3, p_4, p_5) - Rf_{jAve}(X_j, \mu_{y\max} | \{P\})\right\}^2} \quad for\ N_{st} \neq 0 \tag{4}$$

where $N_{st} = N_{st}(X_j, \mu_{ymax})$ is the existing number of $Rf_j^{s,t}$ corresponding to $X=X_j$ and $\mu=\mu_{ymax}$.

3. Statistical properties of fluctuation in seismic response

3.1 Comparison of mean and standard deviation of $Rf_j^{s,t}$

Figure 4(a) shows $Rf_{jAve}(C_b, \mu_{ymax}|\{P\})$ and $Rf_{jStd}(C_b, \mu_{ymax}|\{P\})$, for $X=C_b$. The upper figures are for the condition $\{P\}=\{1,1,1,1,1\}$, i.e., for artificial waves, 1DOF bilinear model with γ=0.001, ΔX_j=0.02, while the lower ones are for the condition $\{P\}=\{1,1,1,2,1\}$, that is, the trilinear model case. In the same manner, the upper figures of Fig. 4(b) show them for $\{P\}=\{1,1,1,1,2\}$, while the lower ones show them for $\{P\}=\{1,1,1,2,2\}$. Considering that $X=C_b$ and ΔX_j=0.02, 0.1 indicates the different rates in P_y, namely, 2% and 10%, respectively.

All the figures of $Rf_{jAve}(C_b, \mu_{ymax}|\{P\})$ seem to depend much more on the level of ductility than on the scale of C_b, although they depend slightly on the scale of C_b in the case of the trilinear model. On the whole, it seems that the larger the level of ductility of the structural responses, the more the difference in the response due to the uncertainty of C_b increases. Concretely, it is outlined that if the ductility stays less than 3.0, the ratio of fluctuation caused by the only 2% difference in P_y is averagely around 0.1 and its standard deviation is around 0.1, and the ratio of fluctuation caused by the 10% difference in P_y is averagely around 0.3 and its standard deviation is around 0.1 or more. The results vary slightly depending on skeleton type. The graph seems to be more complicated for the trilinear model than for the bilinear model.

To compare the characteristics of the mean and the standard deviation of $Rf_j^{s,t}$, the similarity between two graphs was calculated using the following norm:

$$\|W\|_k = \frac{1}{N_u \cdot N_v} \sum_{l=1}^{N_u} \sum_{m=1}^{N_v} \left| W(u_l, v_m | p_1, p_2, p_3, p_4, p_5) - W(u_l, v_m | p_1', p_2', p_3', p_4', p_5') \right|$$

$$(p_i = p_i' \ for\ i \neq k \text{ and } p_i \neq p_i' \ for\ i = k) \tag{5}$$

where W indicates Rf_{jAve} or Rfj_{jStd}, N_u and N_v are the number of discretized u and v, respectively. This norm represents the averaged difference between the two graphs for $Rf_{jAve}(X, \mu_{ymax})$ or $Rf_{jStd}(X, \mu_{ymax})$, the difference caused by the difference in condition p_k. In other words, the $\|W\|_k$ approaches zero if condition p_k has almost no influence on $Rf_j^{s,t}$. Figure 5 shows the $\|W\|_k$ for each condition k. The values for $\|Rf_{jAve}\|_k$ for k=1, 2, and 3 are equal to or less than 0.05; however, some of those for k = 4 exceed 0.1. These results indicate that the pattern of $Rf_{jAve}(C_b, \mu_{ymax})$ possibly varies for different skeleton types; however, it is analogous if the conditions of the input earthquakes, the number of DOFs, and the stiffness ratio are different. On the other hand, the values for $\|Rf_{jStd}\|_k$ are equal to or less than 0.05 for all k. This indicates that the pattern of $Rf_{jStd}(C_b, \mu_{ymax})$ is relatively stable. Further, it means that the Rf_j stably takes values around $Rf_{jAve}(C_b, \mu_{ymax})$. These tendencies of $Rf_{jAve}(C_b, \mu_{ymax})$ or $Rf_{jStd}(C_b, \mu_{ymax})$ for the other conditions $\{P\}$ are basically similar to those shown in Fig. 4. Thus, the basic characteristics of $Rf_j^{s,t}(C_b, \mu_{ymax})$ can be explained by Fig. 4.

As with the above results, Fig. 6(a) shows $Rf_{jAve}(T_1, \mu_{ymax})$ and $Rf_{jStd}(T_1, \mu_{ymax})$, for $X=T_1$. The upper figures show the condition of $\{P\}=\{1,1,1,1,1\}$ and the lower ones that of $\{P\}=\{1,1,1,2,1\}$. The upper figures in Fig.

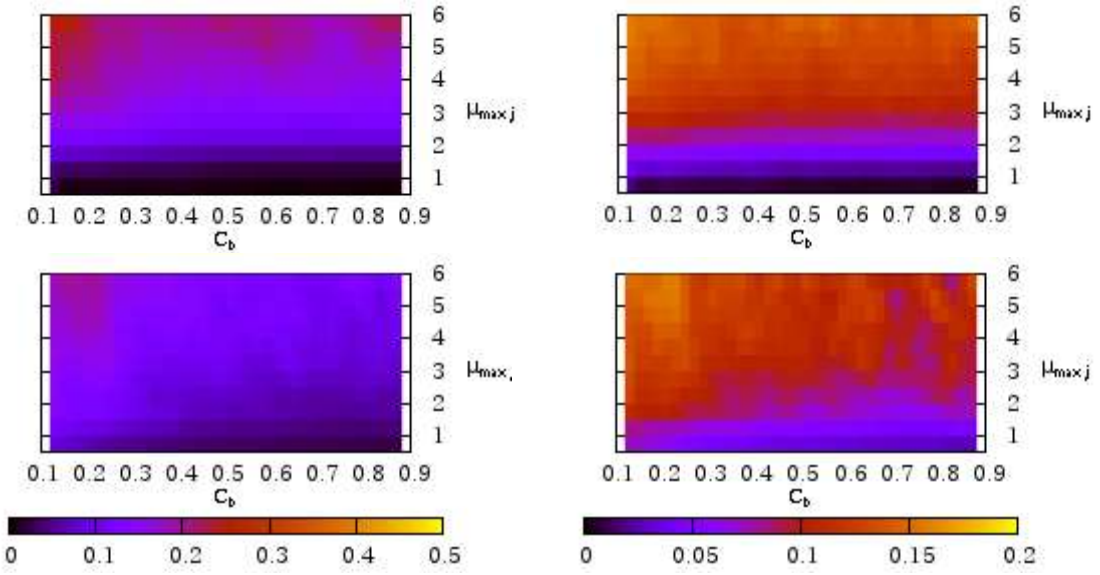

(a) ΔX=0.02

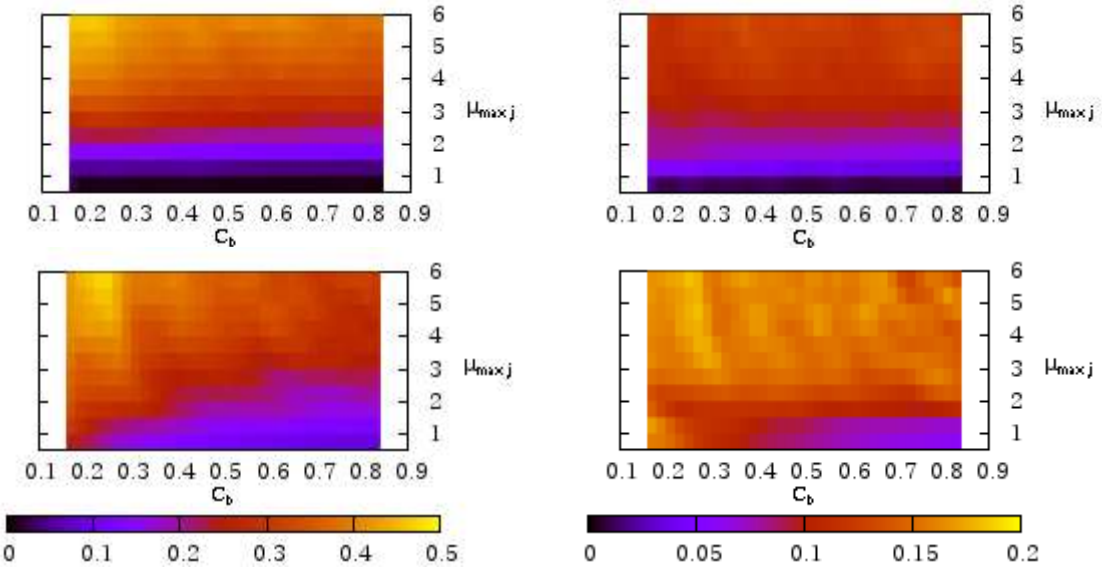

(b) ΔX=0.1

Fig. 4 – Examples of Rf_{jAve} (left) and Rf_{jStd} (right) for $X=C_b$ in the case of the bilinear model (upper) and the trilinear model (lower)

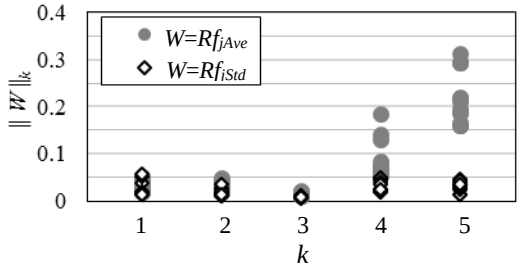

Fig. 5 – Norms with condition parameter k for $X=C_b$

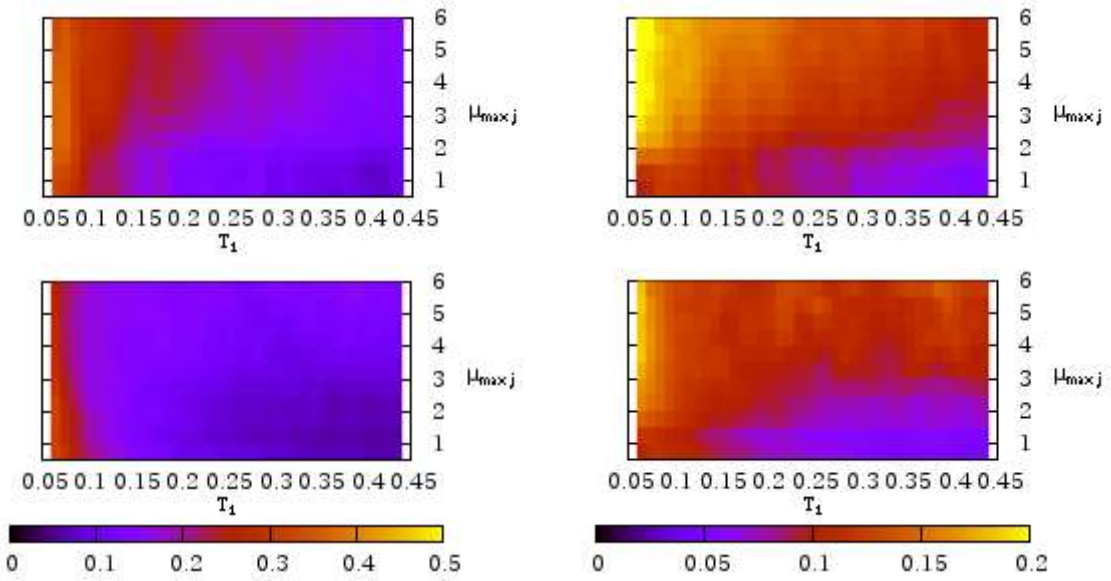

(a) ΔX=0.01

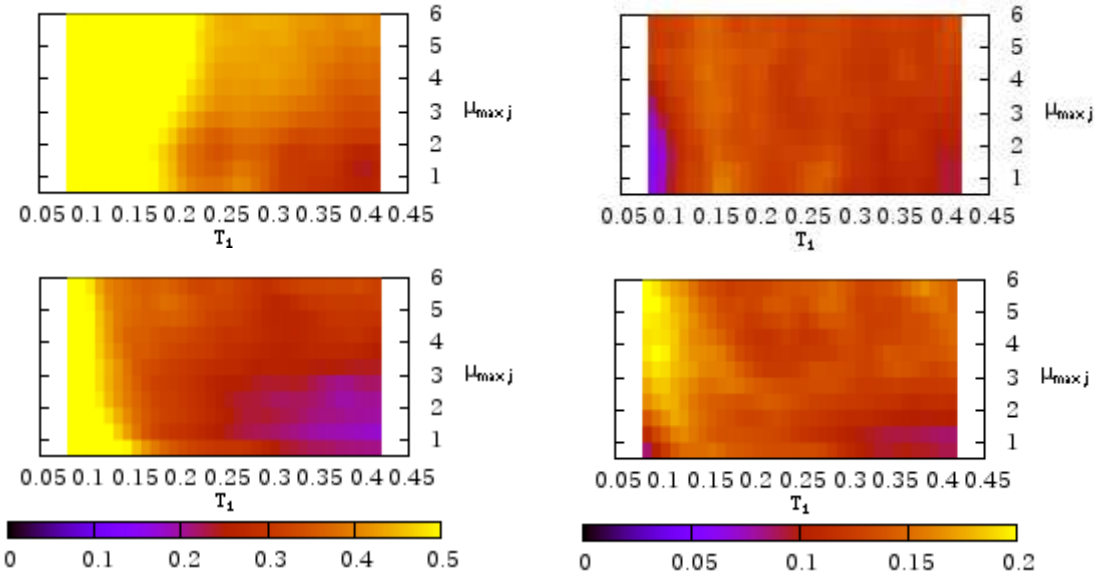

(b) ΔX=0.05

Fig. 6 – Examples of Rf_j for $X=T_1$: The average (left) and standard deviations (right) in the case of the bilinear model (upper) and the trilinear model (lower)

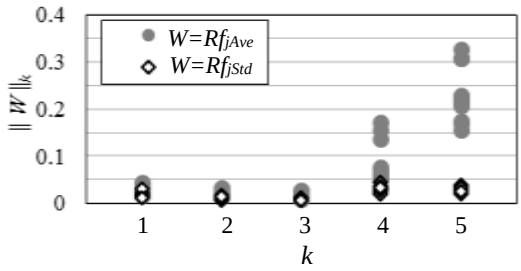

Fig. 7 – Norms with condition parameter k for $X=T_1$

66(b) shows the case of $\{P\}=\{1,1,1,1,2\}$ and the lower ones that of $\{P\}=\{1,1,1,2,2\}$. Considering that $X=T_1$ and ΔX_j=0.01, 0.05 indicates that the difference in T_1 is 0.01 s and 0.05 s, respectively.

Rf_{jAve} (T_1, μ_{ymax}) seems to depend much more on the scale of T_1 than on the level of ductility. One of the causes is that the level of θ_{max} tends to be small if the natural period is short. Then, Rf_j tends to take a large value. The tendency becomes clear with the increase in ΔX_j. Figure 7 shows the $||W||_k$ for each condition k. The tendency of $||W||_k$ is almost the same as that shown in Fig. 5. This result indicates that the characteristics of Rf_{jAve} are analogous to those shown in Fig. 6 if the conditions of the input earthquakes, the number of layers, and the stiffness ratios are different. In addition, all the $||Rf_{jStd}||_k$ take small values. It can be briefly summarized, therefore, that the Rf_j caused only by the difference in T_b of 0.01 s takes a value averagely around 0.1. However, it becomes larger for longer natural periods of structures. Further, it may exceed 0.5 for ΔT_1=0.01 s, which cannot be ignored. Although the standard deviation in $Rf_j^{s,t}$ approaches 0.2 for shorter natural periods, the values are around 0.1. This means that the structural period is not too short and the level of ductility is not too large; $Rf_j^{s,t}$ can approximately be estimated by T_1 and μ_{ymax}.

3.2 Statistical property of Rf_j

Each graph shown in Figs. 4 and 6 consists of 40×16 (p_5=1) or 36×16 (p_5=2) values of Rf_{jAve} or Rf_{jStd}. In other words, these graphs provide us with information on $Rf_j^{s,t}$ by 640 or 576 frequency distributions. The statistical properties of these $Rf_j^{s,t}$ can be useful for evaluating the reliability of the structural responses obtained from the numerical simulation. In this section, the characteristics of the frequency distribution of $Rf_j^{s,t}$ are examined. Examples of the frequency distribution are shown in Fig. 8. Their envelopes seem to be classified as some general distribution patterns. Considering that the $Rf_j^{s,t}$ takes values from 0 to 1, as defined by Eq. (1), the beta distribution seems to be applied to them.

$$p(x)=\frac{x^{\alpha-1}(1-x)^{\alpha-1}}{B(\alpha,\beta)} \quad (0\le x\le 1) \tag{6}$$

where α and β are parameters and $B(\alpha,\beta)$ is the Beta function written by

$$B(\alpha,\beta)=\int_0^1 x^{\alpha-1}(1-x)^{\beta-1}dx \qquad for \;\; \Re(\alpha)>0,\; \Re(\beta)>0 \tag{7}$$

Expected value μ and variance σ^2 of the Beta distribution are represented, respectively, as follows:

$$\mu=\frac{\alpha}{\alpha+\beta} \quad , \quad \sigma^2=\frac{\alpha\beta}{(\alpha+\beta)^2(\alpha+\beta+1)} \tag{8}$$

The χ−square test is applied to 640 or 576 frequency distributions for one calculation pattern, by substituting Rf_{jAve} and Rf_{jStd} into the above μ and σ. For each calculation pattern, the rate of the number of frequency distributions that meets "the significance level of 5%" is calculated and shown in Fig. 9 by a histogram. The total number of calculation patterns is 24 for each X; hence, the total number of histograms is 24. From these figures, although there are some exceptions for X = C_b, the beta distribution totally seems to be applicable to the frequency distribution of $Rf_j^{s,t}$. These results indicate that the unexpected fluctuation in the

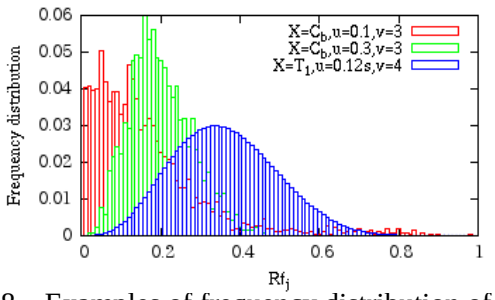

Fig. 8 – Examples of frequency distribution of Rf_j (u, v)

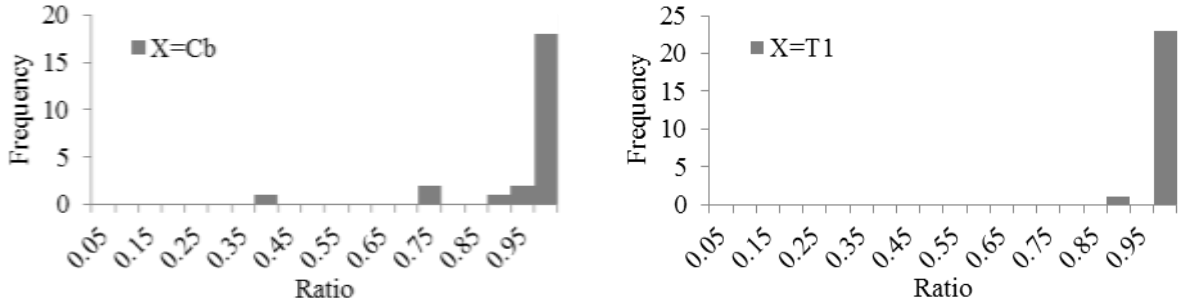

Fig. 9 – Rate of the number of frequency distributions that meets "the significance level of 5%".

response can be explained by certain regular patterns. Thus, these results may possibly become useful information for evaluating the reliability of the numerical results if the reason why the frequency distribution of $Rf_j^{s,t}$ follows the beta distribution is theoretically demonstrated.

4. Summary

To examine the statistical properties of the unexpected fluctuation in the seismic response, accompanied by the uncertainty of structural parameters, the ratio of fluctuation, $Rf_j^{s,t}$, was introduced. Focusing on the maximum story drift angle as the seismic response, the fluctuation in the seismic response was examined through numerical tests using simple shear-spring mass models and a large number of input earthquakes. The statistical properties of $Rf_j^{s,t}$, targeted for the maximum story drift angle, can be summarized as follows: 1) The mean of $Rf_j^{s,t}$ with a slight change in the yield force highly depends on the ductility level. 2) The mean of $Rf_j^{s,t}$ with a slight change in the natural period of the structures depends more on the natural period than on the ductility level. 3) A slight difference in structural parameters, for instance, 2% in the yield force or 0.01 s in the natural period, possibly reaches a difference in story drift angle of around 10% when the ductility is less than 3. 4) $Rf_j^{s,t}$ agrees well with the beta distribution. Further study is necessary to explain these characteristics theoretically.

5. Acknowledgements

The authors thank the Cabinet Office of the Government of Japan for providing the acceleration data for the scenario earthquake (Nankai Trough – Kihon case) used in this study. Provision of the accerelation records observed by K-net during the 2011 Tohoku Earthquake, by the National Research Institute for Earth Science and Disaster Prevention (http://www.kyoshin.bosai.go.jp/kyoshin/), is gratefully acknowledged.

6. References

[1] Bazzurro, P and Cornell, C. Allen: Disaggregation of Seismic Hazard, BSSA, 89, 2, pp. 501-520, 1999.

[2] Baker, Jack W.: Ground motion selection for performance-based engineering, and the conditional mean spectrum as a selection tool, 2015.

[3] Mander, John B. and Basoz, Nesrin; Seismic fragility curve theory for highway bridges, Optimizing Post-Earthquake Lifeline System Reliability, pp. 31-40, 1999.

[4] Fujiwara, H., Kawai, S., Aoi, S., Morikawa, N., Senna S., Kobayashi, K., Ishii, T., Okumura, T. and Hayakawa Y.: National Seismic Hazard Maps of Japan, Bull. Earthq. Res. Inst. Univ. Tokyo, Vol. 81, pp. 221-232, 2006.

[5] Hori, M. and Ichimura, T.: Current state of integrated earthquake simulation for earthquake hazard and disaster, Journal of Seismology, 12(2), pp. 307-321, 2008.

[6] Ichimura, T., Fujita, K., Hori, M., Sakanoue, T. and Hamanaka, R.: Three-dimensional nonlinear seismic ground response analysis of local site effects for estimating seismic behavior of buried pipelines, Journal of Pressure Vessel Technology, American Society of Mechanical Engineers, 136, PVT-13-1131, 2014.